Aust. J. Phys., 1990, **43**, 565–82

Uses of Spin-polarised Electrons in Fundamental Electron–Atom Collision Processes and the Analysis of Magnetic Microstructures*

Michael H. Kelley

Electron and Optical Physics Division, National Institute of Standards and Technology, Gaithersburg, MD 20899, U.S.A.

Abstract

Two experimental programs are discussed which exploit the use of polarised electrons for studies of fundamental processes and physical properties. In one program, collisions between spin-polarised electrons and optically pumped sodium atoms provide a very detailed characterisation of the spin-dependent interactions important in low-energy electron–atom collisions. The results of these measurements provide a critical test for the reliability of state-of-the-art electron scattering calculations. In the second program, the spin polarisation of secondary electrons ejected by high-energy electron impact is used to determine the magnetic structure of ferromagnetic materials with very high spatial resolution (~60 nm). This ability to perform such studies with high resolution has been exploited both in studies of the basic magnetic properties of ferromagnetic materials and in studies of how these basic properties affect the magnetic structure and performance of devices used for magnetic information storage.

1. Introduction

I would like to describe two rather different experimental programs in the Electron Physics Group at NIST which exploit the use of spin-polarised electrons for studies of fundamental physical properties and processes. These programs offer an interesting case study illustrating the value of cross-fertilisation between areas of research which are traditionally considered distinct.

The first program, discussed in Section 2, is the study of collisions between spin-polarised electrons and spin-polarised atoms. These measurements provide one of the most detailed characterisations possible of one of the most fundamental collisional processes. As such, the measurements serve as a benchmark against which to critically judge the accuracy and reliability of theoretical model calculations on which we must rely for the understanding of very many physical processes. This program has been made possible largely through the development both of laser optical pumping, used as a means to study fundamental interactions between light and matter, and of a very efficient source of spin-polarised electrons, initially used for basic studies of the properties of surface magnetism.

* Paper presented at the Workshop on Interfaces in Molecular, Electron and Surface Physics, held at Fremantle, Australia, 4–7 February 1990.

0004-9506/90/040565$03.00

The second program, discussed in Section 3, exploits the development of very efficient electron spin polarisation detectors for microscopic studies of magnetic domain structure. The instrument developed has unique capabilities which allow very high resolution (~60 nm) studies of both basic magnetic properties of materials and the influence of physical structure or materials processing on the magnetic properties of real devices.

2. Electron–Atom Scattering

Collisions between electrons and matter are among the most basic of all physical processes, underlying a very broad range of physical phenomena from electrical resistivity, to gaseous discharges, to the chemistry of the earth's and stellar atmospheres, to energy transport in tokamak plasmas to be used for power generation. Accurate theoretical modelling of electron transport in all such processes is critically dependent both on the theoretical models used and on the availability of reliable electron scattering cross sections. Because it will likely never be possible to determine experimentally all of the scattering cross sections required for the modelling of the full range of scattering processes, one will always have to rely on theoretical calculations for the vast majority of the electron scattering data.

A concern of immediate importance, then, is an assessment of the reliability of data obtained from theoretical electron scattering calculations. At sufficiently high impact energy, where the details of target structure are relatively less important and where the Born approximation may be reasonably accurate, many cross sections are reasonably well calculated. At sufficiently low impact energies, where only a few target states contribute significantly to the collision process, *ab initio* close-coupling calculations are generally expected to provide close agreement between theory and experiment. However, at intermediate energies, from about the threshold for inelastic excitation up to several times the ionisation potential, scattering theory is rather difficult and not quite satisfactory. Because the cross sections for many important scattering processes reach their maximum value in this energy range, it is essential that theoretical models be developed which accurately predict the scattering cross sections.

Collision studies which make use of quantum state preparation and detection techniques have led to a considerable advance in our knowledge of scattering phenomena. In the particular case of electron–atom collisions, substantial progress in the use of coherence, correlation, coincidence, polarisation, optical pumping, and step-wise excitation techniques has made possible experimental investigations which are increasingly detailed in their characterisation of scattering processes (Slevin 1984; Andersen *et al.* 1988; Kleinpoppen 1988; MacGillivray and Standage 1988; Kessler 1985; Hanne 1988; Raith 1988; Kelley 1990). The ultimate goal of such measurements has been the 'complete' or 'perfect' experiments envisioned by Bederson (1969). Such measurements provide the most detailed and complete characterisation possible of the interactions at work in, and the scattering dynamics of, collisions between electrons and atoms. For our measurements, we are interested in making such 'complete' measurements for the effects of exchange in elastic and inelastic electron–atom scattering.

There are two fundamental causes of spin dependence in electron–atom collisions—the spin–orbit interaction and exchange (Kessler 1985). The spin–orbit interaction arises from the interaction of the magnetic moment (spin) of an electron with the magnetic field felt in the rest frame of that electron because of its motion in the electric field of the scattering target. The effective magnetic field is always perpendicular to the scattering plane determined by the momentum of the electron before and after collision. As a result of this effective magnetic field, electrons at a given impact parameter whose spins are 'up' relative to the scattering plane have a different energy from electrons whose spins are 'down'. Hence, the scattering cross section for 'up' electrons is different from that for 'down' electrons. Such scattering is generally referred to as Mott scattering and serves as the basis for essentially all electron spin detectors. Collisional effects arising due to the spin–orbit interaction have been the subject of extensive study and have led to significant improvement in our understanding of collisional processes (Kessler 1985; Hanne 1988). For the present, however, our primary interest is the other fundamental source of spin dependence, exchange, and we will not further discuss collisional effects of the spin–orbit interaction.

Exchange differs from the spin–orbit interaction in that it is not the result of any spin-dependent force at work during the scattering, but is a manifestation of inherent symmetry properties of the wave functions of spin-$\frac{1}{2}$ particles. The simplest system in which to introduce the most important ideas necessary for the understanding of exchange in electron–atom scattering is elastic scattering of spin-polarised electrons from a spin-polarised one-electron atom such as hydrogen, or equivalently, an alkali atom. The ideas we develop are readily applicable to inelastic collisions as well. As we will see, exchange introduces a dependence of the scattering cross section for such systems on the relative orientation of the spins of the incident electrons and atoms. As a result, a measurement of this spin dependence gives one a direct measure of the role played by exchange in these collisions.

In the absence of any spin–orbit interaction, only three non-equivalent scattering scenarios are possible:

$$e(\uparrow) + A(\downarrow) \rightarrow e(\uparrow) + A(\downarrow), \tag{1}$$

$$e(\uparrow) + A(\downarrow) \rightarrow e(\downarrow) + A(\uparrow), \tag{2}$$

$$e(\uparrow) + A(\uparrow) \rightarrow e(\uparrow) + A(\uparrow). \tag{3}$$

Here, the up and down arrows indicate the direction of the electron's and atom's spin polarisation relative to some fixed axis.

In the first example, the spins of both particles remain unchanged, so one can say that no 'exchange' has occurred, and the scattering is characterised by a 'direct' scattering amplitude, f. In the second example, both spins have changed, so 'exchange' has clearly taken place, and the scattering is characterised by the 'exchange' amplitude, $-g$. In the third process, one cannot tell whether the electrons have 'exchanged' or not, so both channels

contribute and the scattering is described by the amplitude, $f-g$, which involves interference between 'direct' and 'exchange' scattering.

While there is a certain attraction to this description of scattering in terms of 'direct' and 'exchange' events, it is advantageous to adopt an alternative description which more clearly reflects one of the most important symmetries of the scattering process, namely that the total spin of the system, electron plus atom, is conserved during the collision. The total spin conservation is emphasised by treating the spin of the colliding electron and atom pair as coupled to form either a singlet or triplet spin state, which is unchanged by the collision. Collisions which take place in either the singlet or triplet state are then fully described by independent singlet and triplet complex scattering amplitudes, S and T, respectively. A complete characterisation of this scattering process thus requires the determination of three parameters, i.e. the magnitudes of S and T and the phase difference between them. Because the cross sections for scattering in the singlet or triplet channel are simply proportional to the squared magnitudes of the amplitudes, those magnitudes can in principle be determined from a measurement of the singlet and triplet scattering cross sections.

The scattering process described in equation (3) is a realisation of the pure triplet state experiment.* Because the initial spins are parallel, only the triplet state is represented and the scattering signal $I_{\uparrow\uparrow}$ is simply proportional to the triplet scattering cross section. That is, $I_{\uparrow\uparrow} \propto \sigma_T = |T|^2$. An absolute determination of that scattering cross section is thus sufficient for a determination of the magnitude of the triplet complex scattering amplitude.

Unfortunately, the singlet state cannot be quite as readily studied. The antiparallel incident spin configurations illustrated in equations (1) and (2) above are described as linear combinations of singlet and triple spin states, and the two scattering scenarios are described by the complex scattering amplitudes $(S \pm T)$. The scattering cross sections for these two processes would be $|S|^2+|T|^2 \pm |S||T|\cos(\phi_{ST})$, where ϕ_{ST} is the relative phase difference between S and T.

If no analysis is performed of the spin of the scattered electrons, then one cannot distinguish between these processes and the cross section for scattering in the initially antiparallel relative spin orientation is just the average of the two cross sections, so that $\sigma_{\uparrow\downarrow} = \frac{1}{2}(\sigma_S + \sigma_T)$.

Notice that there is no sensitivity in either $\sigma_{\uparrow\uparrow}$ or $\sigma_{\uparrow\downarrow}$ to 'interference' between singlet and triplet scattering, and hence no information about the relative phase between S and T. In order to determine that phase difference, one must determine the change in spin polarisation of either the electron or atom which occurs during the collision (Hertel *et al.* 1987). Such experiments have not yet been performed and will not be further discussed here.

Because we are primarily interested in the role of exchange during these collisions, we choose to concentrate not on absolute measurements of the scattering cross sections $\sigma_{\uparrow\uparrow}$ and $\sigma_{\uparrow\downarrow}$ themselves, but on how the cross sections are affected by exchange. We define an exchange asymmetry, A_{ex}, as the

* In this discussion, we assume that both the electrons and atoms are completely polarised and ignore completely any complications arising from incompletely polarised beams. One can fully account for the effects of incomplete polarisation in very straightforward ways, without affecting the present interpretation (Kessler 1985; Hertel *et al.* 1987).

difference between scattering in the initially antiparallel versus initially parallel relative spin orientation, normalised to their sum. That is,

$$A_{ex} = \frac{\sigma_{\uparrow\downarrow} - \sigma_{\uparrow\uparrow}}{\sigma_{\uparrow\downarrow} + \sigma_{\uparrow\uparrow}} = \frac{\sigma_S - \sigma_T}{\sigma_S + 3\sigma_T} . \tag{4}$$

This exchange asymmetry is directly related to the ratio, r, between the triplet and singlet scattering cross sections by

$$r = \frac{\sigma_T}{\sigma_S} = \frac{1 - A_{ex}}{1 + 3A_{ex}} . \tag{5}$$

Either the exchange asymmetry, A_{ex}, or the triplet to singlet ratio, together with an absolute measurement of the absolute scattering cross section, is sufficient for a determination of both $|S|$ and $|T|$.

One important advantage of measuring relative quantities, such as the exchange asymmetry or the cross section ratio, is that one can extract directly from the experiment specific information about the desired effect, in this case exchange, without suffering from the numerous systematic effects which plague measurements of absolute scattering cross sections.

We now turn to a discussion of inelastic scattering processes. Before considering the excitation of a spin-polarised alkali atom by spin polarised electrons, let us first consider how one would describe the excitation process if electrons had no spin. We concentrate on electron induced transitions between S and P states. Because the P state has three degenerate magnetic sublevels, a complete description of this excitation requires, in principle, three complex scattering amplitudes, one for exciting the single S state to each magnetic sublevel of the P state. For the case of $S \rightarrow P$ excitations, and ignoring any influence of the spin–orbit interaction, one can use symmetry considerations to reduce the number of amplitudes. Because the scattering process must preserve the overall positive reflection symmetry about the scattering plane defined by the momentum of the incident and scattered electrons, any angular momentum transferred to the atom must be perpendicular to this plane. We therefore choose to describe the collision in a coordinate system in which the atomic orbital angular momentum is quantised along an axis perpendicular to the scattering plane. In this coordinate system, the amplitude for exciting the $M_L = 0$ magnetic sublevel must vanish. One is thus left with two complex amplitudes, $F_{\pm 1}$, for excitation of the $M_L = \pm 1$ sublevels, respectively.

These amplitudes, including their relative phase, can be determined in an appropriate study of electron impact excitation. Suppose a collision event excites an atom initially in the ground state to the $M_L = +1$ excited state. That excited atom will subsequently emit a photon which, if detected along the direction normal to the scattering plane, has pure circular polarisation. Atoms excited to the $M_L = -1$ sublevel would show the opposite circular polarisation along the same direction. Thus, a measurement of the circular polarisation of the photons emitted normal to the scattering plane, in coincidence with the electron which excited the atom, gives a direct measure of the relative magnitudes of F_{+1} and F_{-1}.

Similar to the approach taken for elastic exchange scattering, we define a relative quantity to characterise the difference between F_{+1} and F_{-1}:

$$L_{\perp} = \frac{\sigma_{+1} - \sigma_{-1}}{\sigma_{+1} + \sigma_{-1}} = \frac{|F_{+1}|^2 - |F_{-1}|^2}{|F_{+1}|^2 + |F_{-1}|^2}. \tag{6}$$

The symbol $L_{\perp}$ is chosen because the measured quantity can be simply interpreted as the net angular momentum, perpendicular to the scattering plane, which is transferred to the atom on excitation to the $3P$ level (Andersen *et al.* 1988).

Of course, collisions seldom leave the excited atom in a pure $M_L = \pm 1$ state. The excited state generally has contributions from both $M_L = +1$ and $M_L = -1$ magnetic sublevels, with their relative contributions determined by the magnitudes of $F_{\pm 1}$. The light emitted normal to the scattering plane, having both + and − circularly polarised components, thus has a linearly polarised component as well. The direction of this linear polarisation is uniquely determined by the phase difference between the excitation amplitudes. Consequently, a determination of that linear polarisation direction, again in coincidence with the scattered electron, is sufficient to determine this phase difference (Andersen *et al.* 1988).

Rather than perform the experiments as described, it is advantageous to perform so-called *superelastic* scattering measurements wherein one first photo-excites the atomic target and then measures the cross section for electron impact de-excitation (Hertel and Stoll 1977). Because the measurement process itself ensures detection only of electrons which have gained the excitation energy of the atoms, and hence are known to have de-excited an excited atom back to the ground state, coincidence techniques are not required. In effect, coincidences between the photon and scattering electron are enforced from the outset, with a subsequent substantial increase in scattering signal. Time reversal symmetry assures us that the measured quantities are identical to those measured with electron–photon coincidence techniques. From the cross section for de-exciting atoms prepared with + and − circularly polarised light, one determines $L_{\perp}$. From the dependence of the scattering signal on the polarisation angle of linearly polarised light, one determines the relative phase between the excitation amplitudes.

The above would be the complete story for $S \rightarrow P$ excitation if electrons had no spin. We now look to what needs to be changed to incorporate spin into the picture. Basically, we need to allow for the excitation of each magnetic sublevel through the independent singlet or triplet spin channels. That is, rather than two complex amplitudes, $F_{\pm 1}$, we require four, $S_{\pm 1}$ and $T_{\pm 1}$, for excitation of the $M_L = \pm 1$ sublevels via the singlet or triplet scattering channels, respectively.

To completely determine four complex scattering amplitudes, to within an arbitrary overall phase, one needs seven real parameters, four to characterise the magnitudes of the scattering amplitudes, and three to characterise three relative phases. Because experiments have not yet been developed to cleanly determine the relative phase differences, we will not discuss them further (Hertel *et al.* 1987). As for the magnitudes, it is convenient to choose the conventional excitation cross section, which is averaged over spin and orbital

angular momentum, and three relative quantities which describe physical aspects of the collision.* We can define the angular momentum transferred perpendicular to the scattering plane in a way similar to that for excitation without spin, but now resolved into singlet and triplet channels:

$$L_{\perp}^{S} = \frac{|S_{+1}|^2 - |S_{-1}|^2}{|S_{+1}|^2 + |S_{-1}|^2}, \tag{7}$$

$$L_{\perp}^{T} = \frac{|T_{+1}|^2 - |T_{-1}|^2}{|T_{+1}|^2 + |T_{-1}|^2}. \tag{8}$$

For the final relative quantity we again choose the ratio of triplet to singlet scattering, but now averaged over angular momentum transferred:

$$r = \frac{\sigma_T}{\sigma_S} = \frac{(|S_{+1}|^2 + |S_{-1}|^2) - (|T_{+1}|^2 + |T_{-1}|^2)}{(|S_{+1}|^2 + |S_{-1}|^2) + 3(|T_{+1}|^2 + |T_{-1}|^2)}. \tag{9}$$

We illustrate these ideas with the results of our measurements at rather low and at intermediate incident energies. The details of the experimental method have been described elsewhere (McClelland *et al.* 1989). Fig. 1 shows results of our measurements of these quantities for spin-polarised superelastic scattering from the $3P$ excited state of sodium at the relatively low incident energy of 2·0 eV. This corresponds to an incident energy of 4·1 eV in the equivalent in elastic scattering process. Measurements of spin dependence inelastic scattering at this low incident energy are not yet available.

Fig. 1*b* shows our experimental results for $L_{\perp}^{S}$ and $L_{\perp}^{T}$. The results for the ratio, r, are shown in Fig. 1*c*. Additionally, the unpolarised $L_{\perp}$ is shown in Fig. 1*a*, along with the experimental results of Hermann *et al.* (1980) at 3 eV incident energy. The theoretical curves in each case are the results of a four-state close coupling calculation by Moores and Norcross (1972) at an inelastic energy of 4·0 eV, corresponding to 1·9 eV superelastic energy. The agreement between theory and experiment, particularly for the ratio r is reasonably good over the entire measured angular range. This agreement is very encouraging and indicative of the accuracy of close coupling methods in this low energy range.

It is interesting, however, to further consider the discrepancy at small angles for $L_{\perp}^{S}$. This inadequacy of the theory is scarcely noticeable in the unpolarised results shown in Fig. 1*a*. The disagreement in the singlet channel is masked in the unpolarised results simply because triplet scattering events are three times more likely than singlet events in an unpolarised experiment. This dramatically illustrates the importance of making measurements that are as complete as possible when striving for the most sensitive possible tests of theoretical predictions.

A recent, but as yet unpublished, seven-state close coupling calculation by Zhou *et al.* (1989) removes essentially all of the discrepancy between the theory and these experimental results. The excellent agreement found for all experimentally determined quantities is a strong indicator of the reliability of this calculational method for this collision process.

* The details for constructing these relative quantities from the experimental scattering signals are given elsewhere and not repeated here (Hertel *et al.* 1987; McClelland *et al.* 1989).

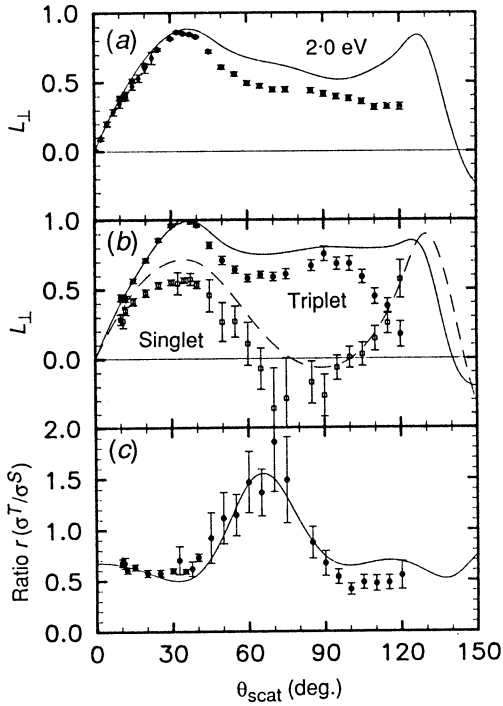

Fig. 1. Spin-polarised superelastic scattering from Na(3*P*) at 2 eV incident energy versus scattering angle θ_{scat}: (*a*) Unpolarised measurement of angular momentum transferred perpendicular to the scattering plane, $L_\perp$. Solid circles from McClelland *et al.* (1989); diamonds from Hermann *et al.* (1980) (3 eV incident energy); solid line, four-state close coupling calculation of Moores and Norcross (1972); (*b*) Singlet (squares) and triplet (circles) perpendicular angular momentum transfer, $L_\perp^S$ and $L_\perp^T$, with calculations of Moores and Norcross (1972) (solid and dashed curves). (*c*) Ratio *r* of triplet to singlet cross sections. Solid circles from McClelland *et al.* (1989); solid line, theory of Moores and Norcross (1972).

Our results for an incident energy of 20·0 eV, about four times the ionisation threshold, are shown in Figs 2 and 3. The 17·9 eV energy for superelastic scattering was chosen to correspond to conventional inelastic scattering at 20·0 eV incident energy.

Fig. 2 shows the elastic exchange asymmetry A_{ex}, which is related by equation (5) to the triplet-to-singlet cross section ratio. It is apparent from the figure that exchange still has an important effect in the elastic scattering channel even at this moderate energy. Over much of the angular range triplet scattering is larger than singlet scattering, by nearly a factor of two in the neighbourhood of 60°. At small angles, the singlet becomes increasingly more important, dominating by about 30% at 20°.

Also shown in Fig. 2 is the exchange asymmetry from a four-state close coupling calculation of Oza (1988). The agreement between theory and experiment is quite good a large angles, but a significant discrepancy is

apparent at smaller angles. The theory predicts a much stronger dominance of triplet over singlet scattering than is seen in the experiment, with this dominance extending essentially down to 0° scattering angle. The source of this disagreement is not at present understood.

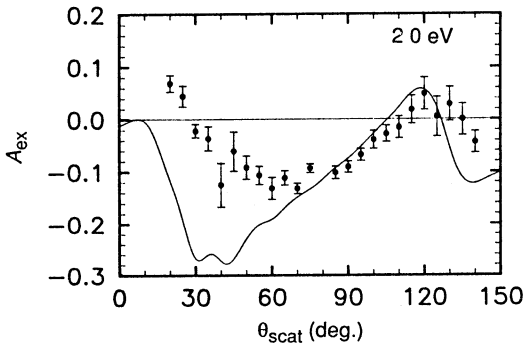

Fig. 2. Exchange asymmetry A_{ex} for elastic scattering from Na at 20·0 eV. Theory is from a four-state close-coupling calculation of Oza (1988).

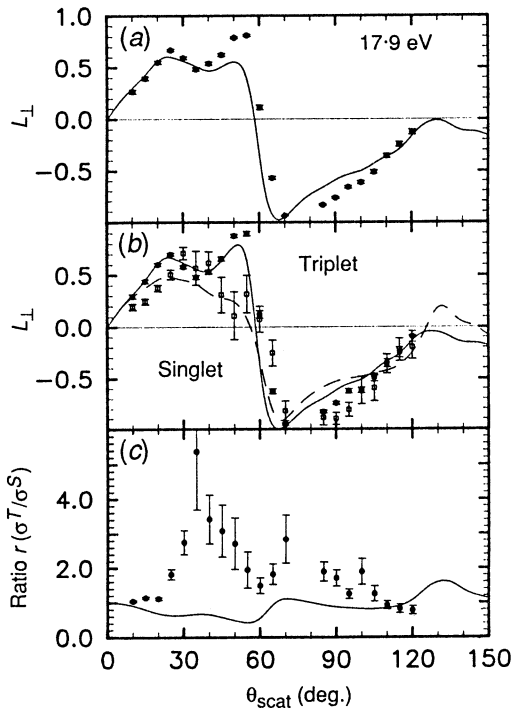

Fig. 3. Spin-polarised superelastic scattering from Na(3*P*) at 17·9 eV incident energy versus scattering angle θ_{scat}: (*a*) Unpolarised measurement of angular momentum transferred perpendicular to the scattering plane, $L_\perp$. (*b*) Singlet (squares) and triplet (circles) perpendicular angular momentum transfer, $L_\perp^S$ and $L_\perp^T$. (*c*) Ratio r of triplet to singlet cross sections.

Our superelastic results for an incident energy of 17·9 eV are shown in Fig. 3. The unpolarised angular momentum transfer, $L_\perp$, is shown in Fig. 3*a*, and the singlet and triplet analogues, $L_\perp^S$ and $L_\perp^T$, are shown in Fig. 3*b*. The triplet to singlet ratio, r, is shown in Fig. 3*c*. The theoretical curves in all cases are the results of a four-state close-coupling calculation by Mitroy *et al.* (1987). As seen from the figure, the theory predicts the angular momentum transfer quite well, but misses the relative importance of singlet and triplet scattering quite severely, indicating that further development of the theory is required.

3. Studies of Magnetic Microstructure

In addition to the uses of polarised electrons in studies of atomic physics, there have been numerous studies of polarised electron scattering and polarised electron emission from ferromagnetic solids (Kessler 1985; Kirschner 1985). In combination with the development and refinement of electron spin polarisation analysers, this work has led to very practical applications for the study of microscopic properties of magnetic materials. The ability to study magnetic properties with high spatial resolution is of both fundamental and technological importance. Magnetic domain structures develop in materials due the delicate balancing of several important contributions to the total energy of a magnetic material. Because the physical parameters which determine the relative sizes of the various energies can vary by several orders of magnitude, the magnetic properties vary widely as well and result in the development of magnetic structures having very different length scales. Such domain structures are often rather complex and can be calculated only for the simplest of systems. Consequently, one must rely on experimental methods for the determination of the details of these magnetic structures.

The study of this domain structure is important not only for furthering our understanding of basic magnetic properties, but for technological reasons as well. For example, the domain structure of a magnetic material is an important consideration in efforts to increase the packing density of information to be stored on high density magnetic recording media. Additionally, the sharpness of transitions between two adjacent domains sets a limit for the signal-to-noise performance of such a media for information retrieval.

On an even finer length scale, one would like to study the detailed structure and dynamics of magnetic domain walls themselves. This is of particular importance for an improved understanding of the magnetic properties of thin films or very small structures to be used as memory elements. As the physical size of such structures is reduced to the same order as the width of a magnetic domain wall, the physical structure can affect the domains and domain wall structure in profound ways.

Clearly, then, an improved ability to study these magnetic properties with high spatial resolution has enormous promise both for developing a better understanding of basic magnetic properties and for improving vital information technologies. We have developed in our laboratory a new method which offers unique capabilities for studying magnetic microstructure. It is based on measuring the spin polarisation of the secondary electrons ejected in a high resolution scanning electron microscope.

Magnetisation arises from the orientation in bulk material of the magnetic moments, or spins, of individual electrons. That is, the magnetisation $\boldsymbol{M}$ is directly proportional to the net spin density, $n_\uparrow - n_\downarrow$, so that

$$\boldsymbol{M} = -\mu_B(n_\uparrow - n_\downarrow), \tag{10}$$

where μ_B is the Bohr magneton and $n_\uparrow$ ($n_\downarrow$) is the number of spins per unit volume parallel (antiparallel) to a particular direction.

Spin polarised electron spectroscopies, for example, photoemission, Auger or secondary electron emission, rely on the fact that this spin orientation is generally not affected by whatever processes eject these electrons from the bulk (Penn *et al.* 1985). Thus a measurement of the free electron spin polarisation can be used as a measure of the net spin orientation in the region from which the electrons originated. Because low energy secondary electrons ejected from transition metal ferromagnets are primarily the result of electron–hole pair creation, and thus reflect the net spin density of the valence band, one can estimate the secondary electron spin polarisation, by

$$P = \frac{n_B}{n}, \tag{11}$$

where n_B is the magnetic moment per atom and n is the number of valence electrons per atom. For iron, cobalt and nickel, one estimates P to be 28%, 19%, and 5%, respectively. The task is to measure this spin polarisation for electrons ejected from a very small source region of a sample.

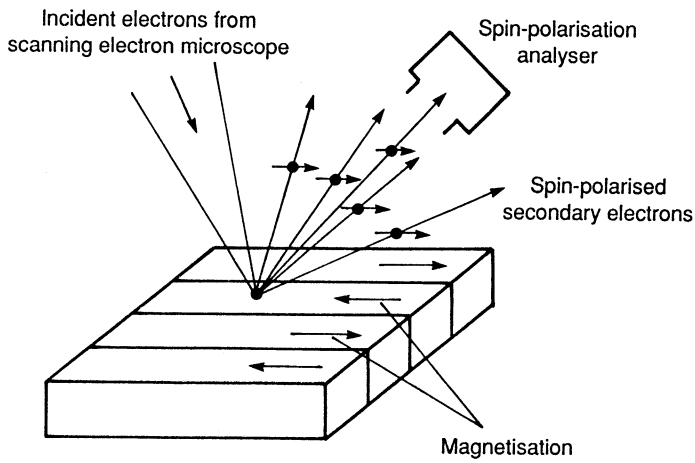

Fig. 4. Principle of scanning electron microscopy with polarisation analysis (SEMPA).

The technique of imaging magnetic microstructure through spin analysis of electrons ejected by a focused high-energy electron beam, illustrated in Fig. 4, has been called scanning electron microscopy with polarisation analysis, or SEMPA (Hembree *et al.* 1987; Koike *et al.* 1987; Celotta and Pierce 1986; Unguris *et al.* 1990). A tightly focused electron beam is rastered across the specimen, continuously generating secondary electrons. The intensity of these secondaries is measured to produce an image of the specimen topography,

familiar as the secondary electron image of scanning electron microscopy (SEM). Additionally, the spin polarisation of these secondary electrons is recorded with an exceptionally compact and relatively efficient spin analyser (Unguris *et al.* 1986; Scheinfein *et al.* 1989*a*) to obtain an image of the magnetic structure. Because we are able to determine the spin polarisation along three orthogonal directions, we can completely reconstruct the three-dimensional orientation of the magnetisation at the surface of the magnetic specimen.

The SEMPA technique has several features which make it a unique tool for the study of magnetic microstructure. First, the spatial resolution is substantially better than for any other currently available technique for studying the magnetic properties of bulk specimens. The resolution in SEMPA is the same as for conventional SEM, with a potential resolution of better than 10 nm. Second, unlike other methods used to study magnetic microstructure, the magnetic information from SEMPA is essentially independent of, but recorded simultaneously with, the topographic information. Consequently, one is able to make detailed studies of relationship between physical and magnetic structures. Third, the polarisation signal and magnetic contrast are large. The secondary electron current can typically be 10–50% of the incident electron beam current, with a typical spin polarisation between 5 and 30%, depending on the specimen. Finally, SEMPA is a surface analytical tool because the secondary electrons have a mean escape depth of only a few nanometres. SEMPA is thus an excellent tool for studies of the magnetic properties of surfaces and thin films.

Shown in Fig. 5 is a typical SEMPA image of the (100) surface of FeSi. The surface was ion-sputtered with a 1 keV argon beam and then reannealed at 700°C. The images are 253 μm across and took about $3\frac{1}{2}$ minutes to acquire. Fig. 5*a* shows the conventional secondary electron intensity image. The surface is relatively smooth and flat, but the existing topological features are clearly visible. The x and y components of the magnetisation vector, M_x and M_y respectively, are shown in Figs 5*b* and 5*c*. In these and all future images, white corresponds to magnetisation in the positive direction, and black to magnetisation in the negative direction. Positive x and y point to the right and up, respectively.

FeSi is characterised by cubic magnetic crystalline anisotropy, so that easy axes of magnetisation, the directions along which the magnetisation points in the lowest energy configuration, are along the cartesian axes. It is also energetically unfavourable to have the magnetisation pointing out of the surface due to the magnetostatic energy which would result. Therefore, on the surface of this or any other cubic anisotropy material, there should be four easy magnetisation axes in the surface, and four principal domain directions. These are clearly seen in Figs 5*b* and 5*c*.

Fig. 5*d* shows the magnitude of the in-plane magnetisation vector, calculated by $|M| = \sqrt{M_x^2 + M_y^2}$. As can be seen, the image is essentially featureless, except for the dark lines decorating the domain boundaries. These lines are artifacts of the measurement and do not indicate that the magnetisation is reduced at the domain walls. Because the probe size used in this measurement was larger than the domain wall, magnetisations of opposing sign from either side of the wall were simultaneously measured, necessarily decreasing the apparent average magnetisation at the boundaries and producing the dark lines in the

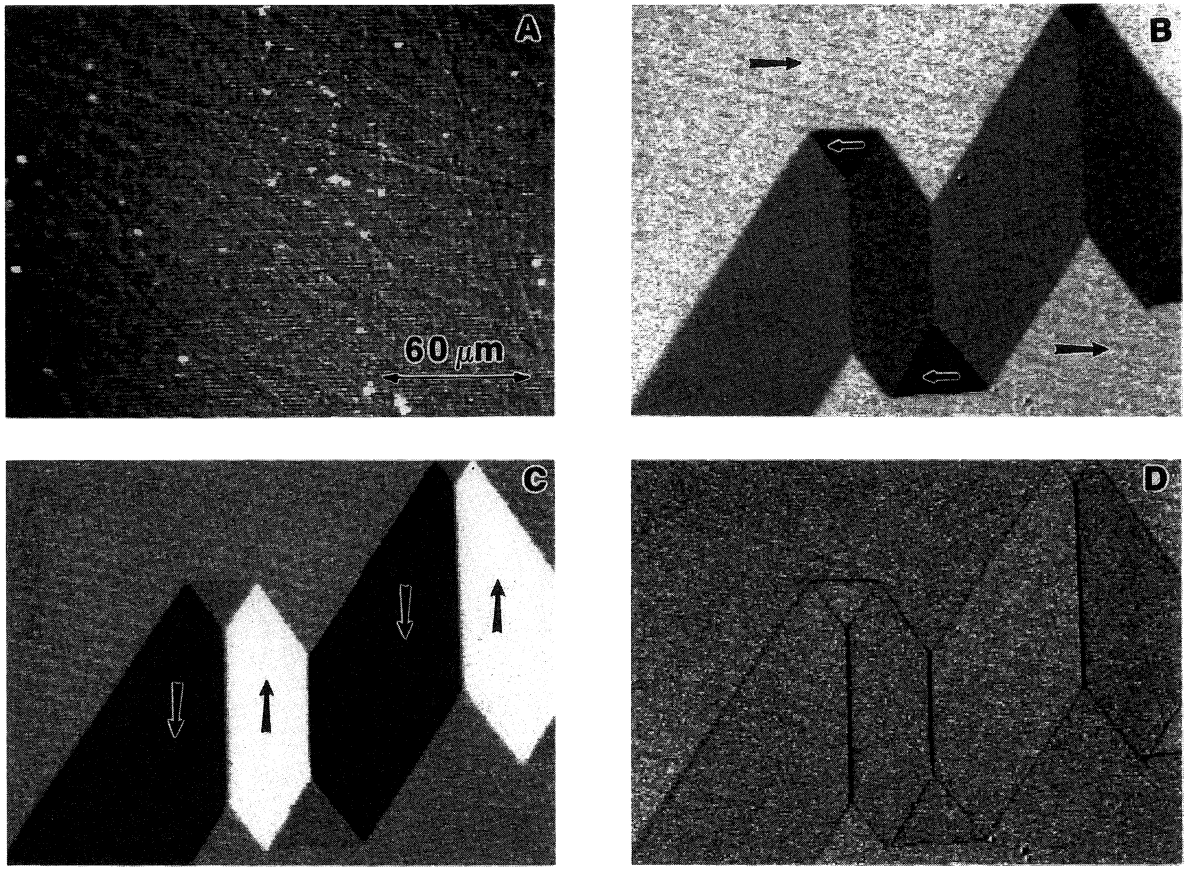

Fig. 5. SEMPA micrograph of the (100) surface of FeSi. The images are 253 μm across. (*a*) Conventional secondary electron image. (*b*) Magnetisation, M_x, along the x direction. (*c*) Magnetisation, M_y, along the y direction. (*d*) Magnitude $|M|$ of the magnetisation.

figure. We have made higher resolution measurements of magnetic domain walls with a probe size sufficiently small that the finite resolution effect is minimised. Such measurements indicate that $|M|$ is constant across the domain wall (Scheinfein *et al.* 1989*b*).

Fig. 6 shows another typical SEMPA image, this one the M_y magnetisation in a (100) face of a single crystalline iron whisker about 125 μm wide and tilted slightly about its long axis. Four magnetic domains are readily apparent in the figure. Because both the x (not shown) and y polarisations are simultaneously measured, one can easily determine the direction of magnetisation in each domain, as indicated by the arrows in the figure. Of particular interest is the depth of field achieved in the SEMPA technique, as indicated by the zig-zag domain wall running down the left side of the whisker.

To illustrate a more practical application of this technique, we next consider an example from magnetic storage technology in which one can correlate performance of the recording media with magnetic domain structure. Information written on magnetic media is typically associated with abrupt transitions in the magnetisation direction of adjacent domains on the media. The noise when reading the media depends critically on the edge acuity between the two opposing domains. One desires the sharpest transition to maximise the signal-to-noise ratio on reading, and the smallest domains to increase the information packing density.

Fig. 7 shows a magnetic test pattern written on a magnetic disk. The active material is a 70 nm thick layer of Co–Ni (approximately 80%–20%). The image displays one component of the magnetisation aligned vertically along the written tracks. The seven vertical bands correspond to successive radial tracks on the disk, and the horizontal domains correspond to the written information.

Fig. 8 shows images at higher magnification of two different magnetic thin film recording media, $Co_{86}Cr_{12}Ta_2$ (Figs 8*a* and 8*c*) and $Co_{75}Ni_{25}$ (Figs 8*b* and 8*d*). Secondary electron intensity images are shown in Figs 8*a* and 8*b*. Clearly visible in each intensity image are grooves in the film surface which are required not for any magnetic properties, but for the mechanical behaviour of recording heads flying very close to the surface. Figs 8*c* and 8*d* show one vertical track of test bits written on the media. In either case, the average track width is about 20 μm and the bit spacing is about $1 \cdot 7$ μm. The magnetic domains are oriented primarily in the direction along the track.

Of particular interest in these images are the primary defects which affect signal-to-noise performance. The $Co_{86}Cr_{12}Ta_2$film shows well separated bits, but with ragged transitions between the domains. The raggedness of the walls, which reduces the sensitivity for determining transitions between the written bits, appears to be correlated with the grooves in the surfaces. The $Co_{75}Ni_{25}$ film clearly shows cross links between neighbouring bits which are also strongly correlated with the topographic structure of the film surface.

Differences between the noise characteristics of the two alloys can be related to the structure of the grain boundaries within the films. In $Co_{75}Ni_{25}$, the Ni forms solid solutions with Co, but in $Co_{86}Cr_{12}Ta_2$, the Cr segregates towards grain boundaries. This effect is enhanced in the presence of Ta, so that the grains in $Co_{86}Cr_{12}Ta_2$ are separated by nonmagnetic boundaries. The magnetostatic and exchange fields are therefore weaker between the grains

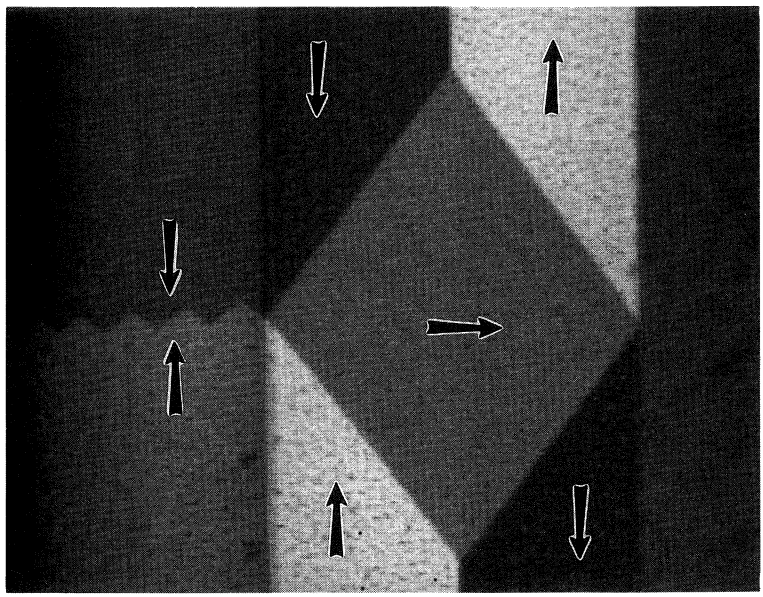

Fig. 6. SEMPA image of the M_y magnetisation of a single crystalline iron whisker, tilted slightly along its long axis. Width of whisker is about 125 μm.

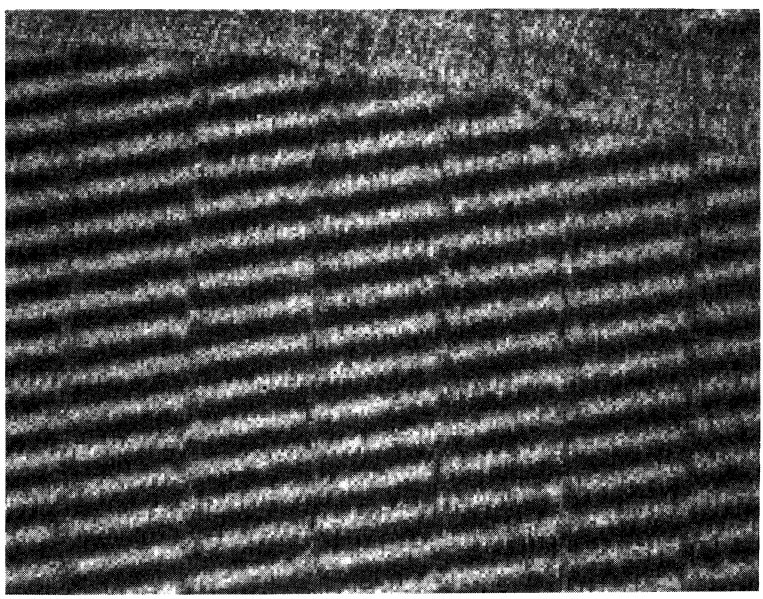

Fig. 7. Written bits in Co–Ni recording media. The seven vertical tracks are approximately 10 μm wide.

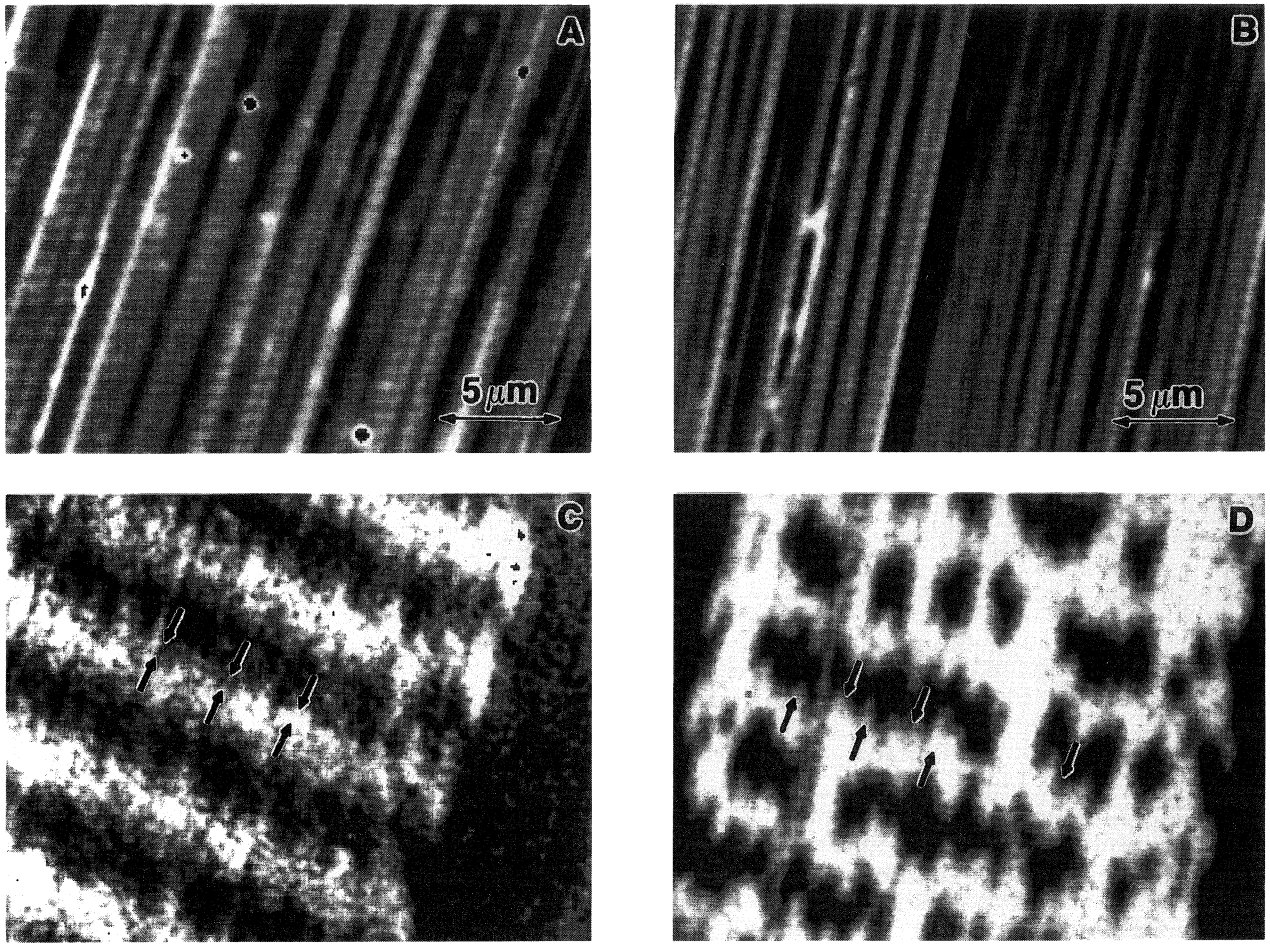

Fig. 8. SEMPA images of two different magnetic recording media: (*a*) secondary image of $Co_{86}Cr_{12}Ta_2$; (*b*) M_y magnetic component of $Co_{86}Cr_{12}Ta_2$; (*c*) secondary image of $Co_{75}Ni_{25}$; (*d*) M_y magnetic component of $Co_{75}Ni_{25}$. In each case, the written bits are about 2 μm wide.

in the $Co_{86}Cr_{12}Ta_2$ film than in the $Co_{75}Ni_{25}$ film. This is supported by the SEMPA results where the cross-bit linkages for $Co_{75}Ni_{25}$ appear much stronger than for $Co_{86}Cr_{12}Ta_2$. These strong cross-bit linkages cause irregularities in the transition between written bits and could account for the reduction in signal-to-noise performance by a factor of about 2·5.

4. Summary

In summary, we have described how spin-polarised electrons can be exploited to investigate very fundamental processes in electron–atom collisions and to investigate basic properties of magnetic microstructure at high resolution.

For the case of electron scattering, we have shown that the best available electron scattering theories are still deficient when examined in detail. Further theoretical development will require more of the detailed measurements of scattering processes made possible with the use of state-selective techniques. As one approaches the final goal of complete measurement of the complex scattering amplitudes and phases, it is expected that electron scattering theory will be significantly improved in its predictive utility.

We have also shown that scanning electron microscopy with polarisation analysis can be a useful tool for the quantitative analysis of magnetic microstructure. Measurements of magnetic properties with high spatial resolution will lead both to a deeper understanding of basic properties of magnetic materials and to a clearer picture of the influence of material characteristics and processing on the magnetic properties of physical devices.

Acknowledgments

I wish to acknowledge the efforts of the participating members of the Electron Physics Group at NIST: R. J. Celotta, D. T. Pierce, J. Unguris, M. R. Scheinfein, and J. J. McClelland. The electron–atom scattering work is supported in part by the U.S. Department of Energy, Office of Basic Energy Sciences, Division of Chemical Sciences. The SEMPA work is supported in part by the Office of Naval Research.

References

Andersen, N., Gallagher, J. W., and Hertel, I. V. (1988). *Physics Reports* **165**, 1.

Bederson, B. (1969). *Comments At. Mol. Phys.* **1**, 41.

Celotta, R. J., and Pierce, D. T. (1986). *Science* **234**, 333.

Hanne, G. F. (1988). *In* 'Coherence in Atomic Collision Physics' (Eds H. J. Beyer, K. Blum, and R. Hippler), p. 41. (Plenum Press: New York).

Hembree, G. G., Unguris, J., Celotta, R. J., and Pierce, D. T. (1987). *Scanning Microscopy Suppl.* **1**, 229.

Hermann, H. W., Hertel, I. V., and Kelley, M. H. (1980). *J. Phys.* B **13**, 3465.

Hertel, I. V., Kelley, M. H., and McClelland, J. J. (1987). *Z. Phys.* D **6**, 163.

Hertel, I. V., and Stoll, W. (1977). *In* 'Advances in Atomc and Molecular Physics', Vol. 13 (Eds D. R. Bates and B. Bederson), p. 113 (Academic Press: New York).

Kelley M. H. (1990). *In* 'Electronic and Atomic Collisions, Invited Papers of ICPEAC XVI' (North-Holland: New York).

Kessler, J. (1985). 'Polarised Electrons', 2nd edn (Springer-Verlag: Berlin).

Kirschner, J. (1985). 'Polarised Electrons at Surfaces' (Springer-Verlag: Berlin).

Kleinpoppen, H. (1988). *In* 'Fundamental Processes of Atomic Dynamics' (Eds J. S. Briggs, H. Kleinpoppen, and H. O. Lutz), p. 393 (Plenum Press: New York).

Koike, K., Matsuyama, H., and Hayakawa, K. (1987). *Scanning Microscopy Suppl.* **1**, 241.

MacGillivray, W. R., and Standage, M. C. (1988). *In* 'Coherence in Atomic Collision Physics' (Eds H. J. Beyer, K. Blum, and R. Hippler), p. 103 (Plenum Press: New York).
McClelland, J. J., Kelley, M. H., and Celotta, R. J. (1989). *Phys. Rev.* A **40**, 2321.
Mitroy, J., McCarthy, I. E., and Stelbovics, A. T. (1987). *J. Phys.* B **20**, 4827.
Moores, D. L., and Norcross, D. W. (1972). *J. Phys.* B **5**, 1482.
Oza, D. H. (1988). *Phys. Rev.* A **37**, 2721.
Penn, D. R., Apell, S. P., and Girvin, S. M. (1985). *Phys. Rev.* B **32**, 7753.
Raith, W. (1988). *In* 'Fundamental Processes of Atomic Dynamics' (Eds J. S. Briggs, H. Kleinpoppen, and H. O. Lutz), p. 429 (Plenum Press: New York).
Scheinfein, M. R., Pierce, D. T., Unguris, J., McClelland, J. J., Kelley, M. H., and Celotta, R. J. (1989*a*). *Rev. Sci. Instrum.* **60**, 1.
Scheinfein, M. R., Unguris, J., Celotta, R. J., and Pierce, D. T. (1989). *Phys. Rev. Lett.* **63**, 668.
Slevin, J. (1984). *Rep. Prog. Phys.* **47**, 461.
Unguris, J., Pierce, D. T., and Celotta, R. J. (1986). *Rev. Sci. Instrum.* **57**, 1314.
Unguris, J., Scheinfein, M. R., Celotta, R. J., and Pierce, D. T. (1990). *In* 'Springer Series in Surface Sciences', Vol. 22 (Springer-Verlag: Berlin).
Zhou, H. L., Whitten, B. L., and Norcross, D. W. (1989). personal communication.

Manuscript received 13 June, accepted 28 June 1990